BOREAL ENVIRONMENT RESEARCH 20: 181–195
ISSN 1239-6095 (print) ISSN 1797-2469 (online)

Helsinki 30 April 2015

Estimating forest leaf area index using satellite images: comparison of *k*-NN based Landsat-NFI LAI with MODIS-RSR based LAI product for Finland

Sanna Härkönen[1)]*, Aleksi Lehtonen[2)], Terhikki Manninen[3)], Sakari Tuominen[2)] and Mikko Peltoniemi[2)]

[1)] *Finnish Forest Research Institute, P.O. Box 68, FI-80101 Joensuu, Finland; *corresponding author's current address: Department of Forest Sciences, P.O. Box 27, FI-00014 University of Helsinki Finland (sanna.harkonen@helsinki.fi)*
[2)] *Finnish Forest Research Institute, P.O. Box 18, FI-01301 Vantaa, Finland*
[3)] *Finnish Meteorological Institute, P.O. Box 503, FI-00101 Helsinki, Finland*

Received 12 Nov. 2013, final version received 17 Sep. 2014, accepted 30 Sep. 2014

Härkönen S., Lehtonen A., Manninen T., Tuominen S. & Peltoniemi M. 2015: Estimating forest leaf area index using satellite images: comparison of *k*-NN based Landsat-NFI LAI with MODIS-RSR based LAI product for Finland. *Boreal Env. Res.* 20: 181–195.

Leaf area index (LAI) is a key variable for many ecological models, but it is typically not available from basic forest inventories. In this study, we (1) construct a high-resolution LAI map using *k* nearest-neighbor (*k*-NN) imputation based on National Forest Inventory data and Landsat 5 TM images (Landsat-NFI LAI), and (2) examine a moderate-resolution LAI map produced based on reduced simple ratio derived from MODIS reflectances (MODIS-RSR LAI). The maps cover all the forested areas in Finland. Country-level averages of Landsat-NFI and MODIS-RSR LAI were at same level, but several geographical and land-use related differences between them were detected. Difference was the largest in the lake district of Finland and in northern Finland, and it increased with decreasing share of forests and increasing share of deciduous trees. As MODIS-RSR LAI does not take into account the sub-pixel variation in land use, Landsat-NFI LAI was found to produce more reliable estimates.

Introduction

The leaf area index (LAI) is one of the key variables used in modeling ecosystem processes, such as carbon uptake. As LAI represents the leaf biomass utilizable in the photosynthesis, it is a good indicator of the canopy health and growing potential of the forest (Stenberg *et al*. 2004). Monitoring of LAI provides important information about the vegetation changes and input data for simulating biological and climatic processes related to forest carbon, nutrient and water balances (Myneni *et al*. 1997, Stenberg *et al*. 2008).

The term 'total LAI' means the one half the total green leaf area per unit ground surface area (one-sided leaf area) (Chen *et al*. 1997). Direct methods for measuring total LAI, such as collecting litterfall, are very laborious and therefore realistic only in some case studies. Instead, utilizing optical sensors or models for producing LAI estimates offer a more relevant tool for practical use (Chen *et al*. 1997). Optical sensors measure 'effective LAI' as a function of canopy gap fraction based on radiation transmission through the canopy (Chen *et al*. 1997). Contrary to total LAI, effective LAI includes the clumping

Editor in charge of this article: Eero Nikinmaa

of needles in the coniferous canopies (Stenberg 1996).

Forest LAI can be measured from the ground either by using optical instruments, such as the LAI-2000 plant canopy analyzer (LI-COR, Lincoln, Nebraska) and Sunfleck Ceptometer (Decagon Devices, Pullman, Washington) (Chen *et al*. 1997) or by deriving it from the basic tree measurements based on allometric relationship between LAI and leaf biomass (Bréda 2003). As these methods are applicable only within ground-based inventories, remote-sensing based methods have been developed for large-scale monitoring of LAI (e.g. Myneni *et al*. 2002, Fernandes *et al*. 2003). Satellite images can be utilized for LAI estimation either by applying empirical regressions based on e.g. vegetation indices, or physically based methods, which are based on forest reflectance models (Curran and Steven 1983, Clevers 1988). In addition to novel methods to utilize reflectance models for LAI estimation (e.g. Heiskanen *et al*. 2011), the light detection and ranging (LiDAR) data have also been successfully used to estimate LAI in the recent years based on the proportion of pulses that hit the vegetation of all the pulses (e.g. Lefsky *et al*. 1999, Lee *et al*. 2009, Korhonen *et al*. 2011).

Accuracy of LAI estimates may vary depending on e.g. the tree species, forest structure and timing of the measurement (Majasalmi *et al*. 2013). For example optical methods tend to underestimate LAI in coniferous forests because of clumping of needles (Stenberg 1996). LAI also varies seasonally and according to Rautiainen *et al*. (2012) the boreal broadleaved and mixed stands reach their maximal leaf area by mid-July, while the coniferous and seedling stands reach maximum LAI in late August.

Several remote-sensing-based LAI products in different resolutions are available for research purposes. For example, the moderate resolution imaging spectroradiometer (MODIS) product is based on the TERRA satellite, which was launched in 2000, provides worldwide LAI estimates with 1-km resolution (Myneni *et al*. 2002). Even though the existing moderate-resolution satellite images are widely used for estimating LAI at regional scale, the pixel-level estimates can be biased especially in the areas, where the land-use structure is very fragmented. For example high share of water bodies can have a remarkable influence on reliability of LAI estimates. Further, MODIS LAI is strongly affected by the understory vegetation (Tian *et al*. 2002, Wang *et al*. 2004), which has an effect on its seasonal reliability in boreal forests (Heiskanen *et al*. 2012, Rautiainen *et al*. 2012). A relevant remote-sensing based alternative for producing canopy LAI maps is to use empirical relationships of LAI and reflectance-based spectral vegetation indices, such as reduced simple ratio (RSR), which is considered to reduce effects of understory vegetation (Stenberg *et al*. 2004). Another approach is to generalize LAI estimates derived from the ground inventories into wall-to-wall maps by using e.g. *k* nearest-neighbor (*k*-NN) imputation based on satellite images. This kind of multi-source forest inventory method has successfully been applied for estimating basic forest variables, such as mean height and stand biomasses (Tomppo *et al*. 2008).

In this study, we examined feasibility of producing a high-resolution wall-to-wall LAI map based on National Forest Inventory (NFI) data, allometric equations and Landsat 5 TM images (30-m resolution) covering all the forested areas in Finland (referred as Landsat-NFI LAI from now on). Subsequently, the produced LAI map was compared with a moderate-resolution LAI product developed for Finland based on RSR calculated form MODIS reflectances (referred as MODIS-RSR LAI) as well as with an original MODIS LAI map. In the Landsat-NFI method, LAI is first estimated for the NFI sample plots and then imputed for all the forested pixels using the *k*-NN estimation method on the basis of Landsat images. The main goal was to investigate effects of different land uses, forest types and geographical location on the Landsat-NFI and MODIS-RSR LAI estimates. For comparison, we also examined RSR-based LAI estimation using Landsat 5 TM images.

Material

NFI data

The LAI estimates were first calculated for the Finnish National Forest Inventory (NFI) plots

Table 1. Summary statistics from the reference NFI data used in *k*-NN imputation for producing the Landsat LAI maps.

	Foliage biomass (kg ha^{-1})	Effective LAI (m^2 m^{-2})	Age (years)	Height (m)	Basal area (m^2 ha^{-1})
MINERAL SOILS (*n* = 21571)					
Min.	70.3	0	1	1.5	1.0
Mean	5291.6	2.2	62	15.6	18.1
Max.	22542.0	10.4	448	33.3	67.0
PEATLANDS (*n* = 7747)					
Min.	48.84	0.1	2	1.5	1
Mean	4235.4	2.1	71	13.6	16.7
Max.	23242.9	12.0	287	29.2	48

measured during 2004–2008 (http://www.metla.fi/ohjelma/vmi/vmi10-info-en.htm) (Table 1). The LAI estimation method is described in the chapter 'Estimating LAI based on NFI data and *k*-NN imputation with Landsat 5 TM satellite images'. A total of 29 319 sample plots were included in the analysis, of which 21 572 were mineral soil forests, the rest being peatland forests. Only the plots, which were located within a single stand and where the productivity was > 1 m^3 ha^{-1} year^{-1}, were selected for the analysis.

The sample plots were truncated angle-gauge plots, which were located systematically in clusters. In southern Finland the distance between the clusters was 6–8 km, the maximum radius 12.52 m and each cluster contained 18 plots. In northern Finland the grid was sparser, the distance between the clusters was 6–11 km, the maximum radius 12.45 m and each cluster contained 14 plots. The plots were located 300 m apart.

The tally trees were selected with a relascope coefficient of 2 in southern Finland and 1.5 in northern Finland. Diameters and tree species were determined for the tally trees. Total tree heights and crown base heights were measured for the sample trees (every 7th tree in the whole inventory).

Tree heights and crown-base heights for all the tally trees were estimated using a multivariate linear mixed-effects model with species-specific parameters designed for multi-response NFI data (Eerikäinen 2009). The NFI data used in the study contained also stand basal area (BA, m^2 ha^{-1}), stand crown coverage (%), site type (Cajander 1925) and tree species.

Processing of satellite images

Landsat 5 TM images

Landsat 5 TM images (http://landsat.gsfc.nasa.gov/) (radiometrically and geometrically corrected) were utilized in the *k*-NN imputation. Most of the images were captured in summer 2007, except for few areas in the north, for which images from 2004–2006 were used, as cloud-free images from 2007 were not available (Table 2). The images were georeferenced to the Finnish uniform coordinate system using the ArcGIS software. Clouds were masked out using the Grass GIS (http://grass.osgeo.org/) *i.landsat.acca* function (Irish 2000, Irish *et al*. 2006). Only the pixels defined as productive forests (growth > 1 m^3 ha^{-1} year) based on land use map

Table 2. Landsat 5 TM and MODIS images used in the study.

	Path/rows	Date of capture
Landsat image		
1–4	188/15, 16, 17, 18	4 Jun. 2007
5–9	190/14, 15, 16, 17, 18	2 Jun. 2007
10–11	191/11, 12	25 Aug. 2006
12–14	186/16, 17, 18	9 Aug. 2007
15–16	191 16, 18	9 Jun. 2007
17–18	190/12, 13	4 Jul. 2007
19	193/13	23 Aug. 2006
20	193/12	1 Aug. 2004
21	188/15	14 Jun. 2005
22	188/14	20 Aug. 2006
MODIS image	Name	Date of capture
1	QKM_1039	2 Jun. 2007
2	HKM_1039	2 Jun. 2007

by Finnish multi-source NFI (MS-NFI) (Tomppo *et al*. 2008, Tomppo *et al*. 2012) were included in the analysis.

The Landsat images were atmospherically corrected using dark object subtraction (DOS) method, where the darkest objects (e.g. water bodies) in the scene are used for calibrating the images (Chavez 1996). Atmospheric correction was done with the DOS_2 method (Song *et al*. 2001). Atmospheric correction was conducted to obtain surface reflectances for calculating spectral vegetation indices such as the reduced simple ratio.

MODIS images

Two cloud-free MODIS images were available in Finland in summer 2007 (Table 2). The atmospheric correction was carried out by the Finnish Environmental Institute (SYKE) using their standard procedure (Rahman and Dedieu 1994). Then the image was georeferenced to the Finnish uniform coordinate system using the Ermapper software. The CORINE land cover map of 2006 (Törmä *et al*. 2008) was used for calculating the forest fraction of each MODIS pixel at 500-m resolution. Only the pixels, with the forest fraction of > 0.5 were selected for the analysis.

Methods

Estimating LAI based on NFI data and *k*-NN imputation with Landsat 5 TM satellite images

LAI estimates for the NFI sample plots

Leaf area indices were first estimated for the NFI plots and then imputed for all the forested areas in Finland (excluding the northernmost Lapland). Total LAI (m^2 m^{-2}) can be expressed based on stand leaf biomass, W (kg DW ha^{-1}), and specific leaf area, S (m^2 kg^{-1}), as

$$L = W \times S/10000. \quad (1)$$

In reality, the specific leaf area is not constant, but it varies according to, e.g., tree species and light conditions. We calculated total LAI using species- and light status-specific parameters as:

$$L_S = \sum_{i=1}^{3} \frac{\left(W_{i,\mathrm{sun}} S_{i,\mathrm{sun}} + W_{i,\mathrm{shade}} S_{i,\mathrm{shade}}\right)}{10000}, \quad (2)$$

where $W_{i,\mathrm{sun}}$ is the leaf biomass of sun leaves and $W_{i,\mathrm{shade}}$ is the leaf biomass of shade leaves in the stand (kg DW ha^{-1}) and i denotes the tree species (1 = Scots pine, 2 = Norway spruce and 3 = birch). $S_{i,\mathrm{sun}}$ and $S_{i,\mathrm{shade}}$ are parameters for specific leaf areas of species i in sun and shade leaves, respectively (*see* Table 3).

Tree-wise leaf biomass for conifers was estimated using multivariate biomass equations for Scots pine (Repola 2009), Norway spruce (Repola 2009) and birches (Repola 2008), in which the independent variables were tree diameter, height and living crown length. The birch biomass model was applied to all deciduous trees.

The tree-wise leaf biomasses were classified into sun and shade leaves based on their location in the canopy according to Stenberg *et al*. (1998), which reports that the specific leaf area of conifers varies depending on the canopy openness. In the stands, where the measured canopy cover was > 50% (with Norway spruce stand > 70%), the leaves located below the vertical mid-point of the stand basal-area-median-tree's crown in

Table 3. Parameters for specific (total) leaf area.

	SLA of sun leaves (m^2 kg^{-2})	SLA of shade leaves (m^2 kg^{-2})	Source
Scots pine	12.5	15.0	Stenberg *et al.* 2001, Palmroth *et al.* 1999
Norway spruce	8.0	11.0	Stenberg *et al.* 1999
Birch	28.0	28.0	Lintunen *et al.* 2011, Sellin & Kupper 2006, Parviainen *et al.* 1999

the canopy were considered shade leaves, the rest being considered sun leaves. Otherwise all the leaves were treated as sun leaves.

The parameters for specific leaf area of Scots pine (*Pinus sylvestris*), Norway spruce (*Picea abies*), and birches (*Betula* spp.) were adjusted based on literature data (Stenberg *et al*. 2001, Palmroth *et al*. 1999, Stenberg *et al*. 1999, Lintunen *et al*. 2011, Sellin *et al*. 2006, Parviainen *et al*. 1999). Birch parameters were applied to all deciduous trees, as majority (81%) of all the deciduous trees in Finland are birches (Finnish Forest Research Institute 2010).

In order to compare the Landsat-NFI LAI estimates with those of MODIS-RSR LAI, total all-sided Landsat-NFI LAI was converted to one-sided effective LAI, L_E, by applying clumping factor for conifers (c_C = 0.57, Stenberg 1996), and conversion factor from all-sided to one-sided (c_S = 0.5) as:

$$L_E = [(L_{S,\text{Scots pine}} + L_{S,\text{Norway spruce}})c_C + L_{S\ \text{deciduous}}]c_S \quad (3)$$

k-NN imputations for all the forested Landsat pixels

The *k*-NN imputations were conducted using image-wise teaching data sets, which were created by linking LAI estimated for the NFI sample plots with the Landsat 5 TM pixel values (bands 1–5 and 7) at those plots. The pixel values were extracted from the Landsat images based on the sample plot midpoint. The nearest neighbors for each satellite image pixel were searched in terms of similarity in the image bands using Euclidian distance. The final maps were produced with k = 1 to represent the same variation in the pixel values as in the measured data, and because the data were later aggregated to pixels comparable to MODIS pixels. This means, that each forested satellite-image pixel was given a LAI estimate of the most similar neighbor available in the teaching data set. The *k*-NN imputations were done using the *yaImpute* package in R (Crookston and Finley 2008, http://www.r-project.org/).

The imputations were run separately for each Landsat image (*see* Table 2) and separately for mineral soils and peatlands (e.g. as Härkönen *et al*. 2011). The imputations were done only for the pixels, which were defined as productive forests (growth > 1 m^3 ha^{-1} per year) in the forest class map from MS-NFI (Tomppo *et al*. 2008, Tomppo *et al*. 2012). The mineral soil and peatland maps were first combined together in the Landsat image blocks. The blocks were then merged to cover whole country at 30-m resolution. In order to compare the Landsat-NFI LAI with the MODIS-RSR LAI estimates, the Landsat-NFI LAI map was resampled to the same 500-m resolution. Thus, the final Landsat-NFI LAI map in 500-m resolution contained average LAI of the forested pixels. Maps were processed using ArcGIS and Grass GIS tools.

Estimating LAI based on reduced simple ratio

The reduced simple ratio (RSR) index (Brown *et al*. 2000), has been reported to correlate well with LAI in boreal coniferous forests (Stenberg *et al*. 2004). The RSR is calculated as

$$\text{RSR} = \frac{\rho_{NIR}}{\rho_{red}}\left(\frac{\rho_{SWIRmax} - \rho_{SWIR}}{\rho_{SWIRmax} - \rho_{SWIRmin}}\right), \quad (4)$$

where ρ_{red} is the red (620–670 nm), ρ_{NIR} is the near infrared (841–876 nm) and ρ_{SWIR} is the short wave infrared (1628–1652 nm) reflectance. $\rho_{SWIRmax}$ and $\rho_{SWIRmin}$ are the maximum and minimum reflectances of the short wave infrared channel.

MODIS-RSR LAI was estimated using equation, which had been originally fitted based on the RSR from a SPOT HRVIR image (acquired 2 August 2003) and terrestrial LAI in central Finland by Stenberg *et al*. (2008) as:

$$\text{LAI} = 0.52\text{RSR} - 0.4 \quad (5)$$

For MODIS images the minimum (0.01%) and maximum (24.29%) reflectance values were derived as the minimum and maximum reflectance values of the SWIR channel for pixels, where the simple ratio (ρ_{NIR}/ρ_{red}) exceeded 6 (Stenberg *et al*. 2008). Only pixels for which more than 50% of the area was forested, according to the CORINE land cover map 2006 (Törmä *et al*. 2006), were used in the analysis.

For comparison, the RSR was calculated for the NFI plots also using the Landsat 5 TM images. Minimum and maximum reflectances for a SWIR channel were determined from the SWIR values in the NFI plots located in the corresponding image.

The red, NIR and SWIR channels of SPOT, Landsat and MODIS are spectrally sufficiently similar to justify the use of the same coefficients for LAI estimation on the basis of the RSR for both image types (SPOT: red 610–680 nm, NIR 790–890 nm and SWIR 1580–1750 nm; MODIS: red 620–670 nm, NIR 841–876 nm and SWIR 1628–1652 nm; Landsat 5 TM: 630–690 nm, 750–900 nm and 1550–1750 nm).

Statistical analysis

As the leaf area indices were not measured in the field, reliability of the imputed LAI maps could not been assessed directly. We examined level of LAI estimates by regressing the Landsat-based RSR with LAI estimated for the NFI plots in Puumala and Suonenjoki, and compared the results with those of the previous study conducted in the same regions by Stenberg *et al.* (2004). Further, we evaluated NFI-based imputations by comparing the imputed and measured plot-level stand basal areas (m^2 ha^{-1}) using leave-one-out cross-validation (LOOC). In LOOC the estimates are imputed for each pixel in the reference data set (i.e. the NFI plots) based on the reference teaching data set (excluding the current plot), and the imputed values are compared with the field reference ones. The basal area imputations were assessed with absolute and relative root mean squared errors (RMSE), and the absolute and relative model biases (Table 4).

Table 4. Statistical equations used in the analysis; y_i is the reference value in a plot i, $\hat{y}_i$ is the k-NN-imputed value in a plot i, $\overline{y}$ is the arithmetic average of the y values, and n is the total number of the plots.

Statistics	Equation
Root mean squared error	$\mathrm{RMSE} = \sqrt{\frac{\sum_{i=1}^{n}(y_i - \hat{y}_i)^2}{n}}$
Relative root mean squared error	$\mathrm{RMSE\%} = \frac{\mathrm{RMSE}}{\overline{y}} \times 100$
Absolute bias	$\mathrm{BIAS} = \sum_{i=1}^{n}\frac{(y_i - \hat{y}_i)}{n}$
Relative bias	$\mathrm{BIAS\%} = \frac{\mathrm{BIAS}}{\overline{y}} \times 100$
Degree of determination	$r^2 = 1 - \frac{\sum_{i=1}^{n}(y_i - \hat{y}_i)^2}{\sum_{i=1}^{n}(y_i - \overline{y}_i)^2}$

Maps produced by MS-NFI (30-m resolution) were used for calculating fractions of different land uses and forest types in the 500-m MODIS pixel. The following variables were calculated based on the MS-NFI maps: fraction of productive forests (land-use class 1), fraction of water, fraction of agricultural land, fraction of buildings and roads, and fraction of different tree species (Scots pine, Norway spruce, birch). Further, the relative standard deviation of the Landsat-NFI-LAI estimates in the MODIS pixel was calculated. The raster calculations were carried out using GRASS GIS (http://grass.osgeo.org/). The statistical analyses was conducted using R (http://www.r-project.org/). Normality of the variables was tested visually by examining histograms. One-way ANOVA was applied to compare differences between the land-use classes.

Results

The canopy LAI estimates produced using the NFI data and the Landsat 5 TM images (mean LAI = 1.94) were on average at the same level as those produced based on MODIS images (average LAI = 1.89). However, the MODIS-RSR LAI estimates had wider range (0–7.4) than Landsat-NFI LAI (0.15–4.9) (Fig. 1). The MODIS-RSR LAI estimates had much larger proportion of very low LAI estimates especially in the conifer-dominated pixels, than the Landsat-NFI LAI estimates (Fig. 2). The MODIS-RSR LAI estimates were generally lower in northern Finland and higher in southeastern Finland, than those produced using NFI and Landsat data. MODIS-RSR LAI and Landsat-NFI LAI were in best agreement in the western part of Finland (Fig. 3). Comparison with the original MODIS LAI product (from 2 June 2007) showed that original MODIS LAI was remarkably higher

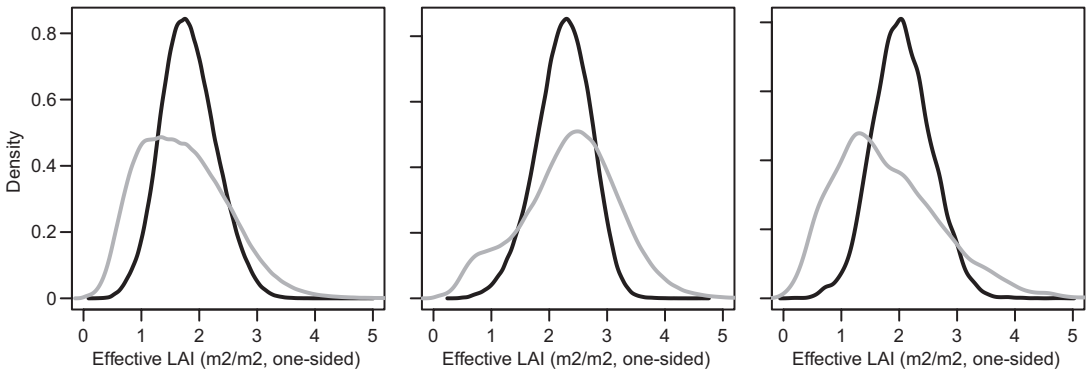

Fig. 1. Distribution of Landsat-NFI LAI (resampled to 500-m resolution) (black) and MODIS-RSR LAI (500-m resolution) (grey) classified according to the dominant tree species (> 50% share of the stem volume in the pixel): Scots-pine- (left, n = 394 464), Norway-spruce- (middle, n = 90 144) and deciduous-tree- (right, n = 1089) dominated pixels. The pixels include only those, where the forest fraction was > 0.5.

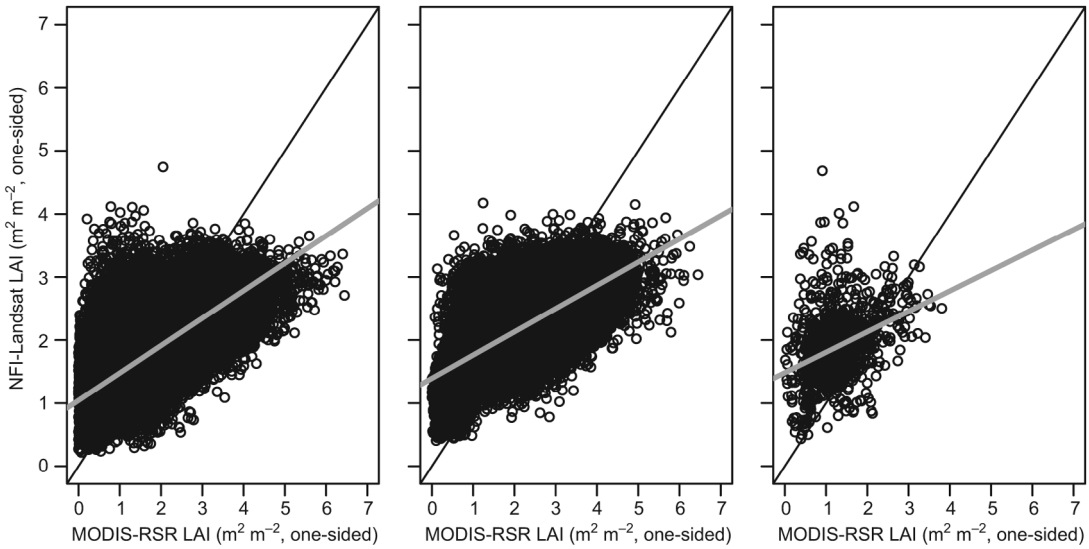

Fig. 2. MODIS-RSR LAI *vs.* Landsat-NFI LAI in Scots pine dominated pixels (y = 1.04 + 0.43x, r^2 = 0.46, n = 394 464, p < 2.2e–16) (left), Norway spruce dominated pixels (y = 1.39 + 0.37x, r^2 = 0.41, n = 90 144, p < 2.2e–16) (middle) and deciduous dominated pixels (y = 1.48 + 0.32x, r^2 = 0.13, n = 1089, p < 2.2e–16) (right).

than Landsat-NFI LAI and MODIS-RSR LAI, except at the highest latitudes (Fig. 4). MODIS RSR LAI and original MODIS LAI followed a similar latitudinal pattern, while the latitudinal differences were smaller with Landsat-NFI LAI.

Difference between the MODIS-RSR and Landsat-NFI LAI estimates varied along land-use fractions in MODIS pixels. Statistically significant differences were detected between groups classified by fractions of forests ($F_{1,748015}$ = 76 835, p < 2e–16), deciduous trees ($F_{1,78015}$ = 40.46, p = 2e–10), water ($F_{1,78015}$ = 654.1, p < 2e–16) and agricultural land ($F_{1,78015}$ = 12956, p < 2e–16) in the MODIS pixel. The difference between MODIS-RSR LAI and Landsat-NFI LAI decreased with increasing proportion of forests in the area (Fig. 5), while high proportion of deciduous trees increased the difference between the MODIS- and NFI-based LAI estimates. The Landsat-NFI LAI estimates for birch-dominant pixels were greater than those estimated by MODIS-RSR. In order to examine reasons behind the differences in the LAI products, we regressed MODIS-RSR LAI, Landsat-

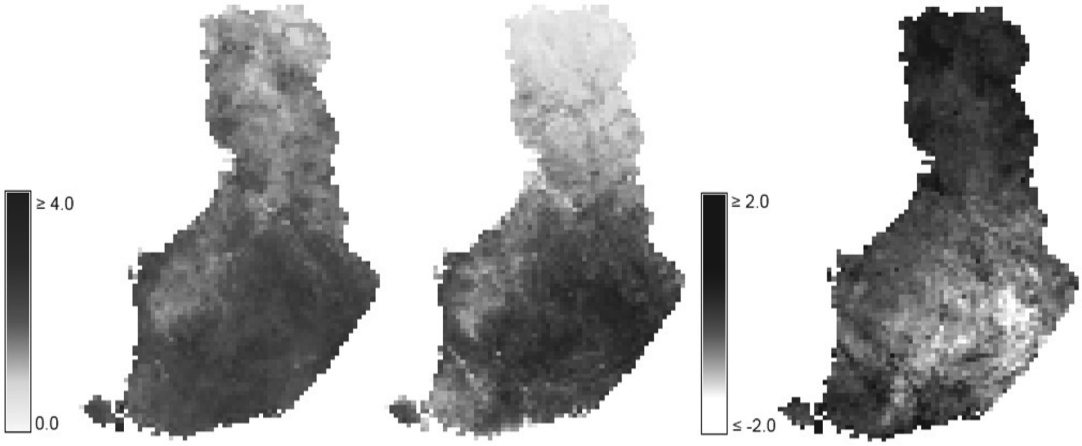

Fig. 3. Maps of Landsat-NFI LAI (left), and MODIS-RSR LAI (middle) and their difference (Landsat-NFI LAI – MODIS-RSR LAI) (right) in Finland resampled to the 10 × 10 km grid. The scale bar (m^2 m^{-2}) on the left is for the two LAI maps, and the scale bar (m^2 m^{-2}) on the right is for difference map next to it. Northermost Lapland is not included, due to fact that it was not measured during the NFI10 field campaign.

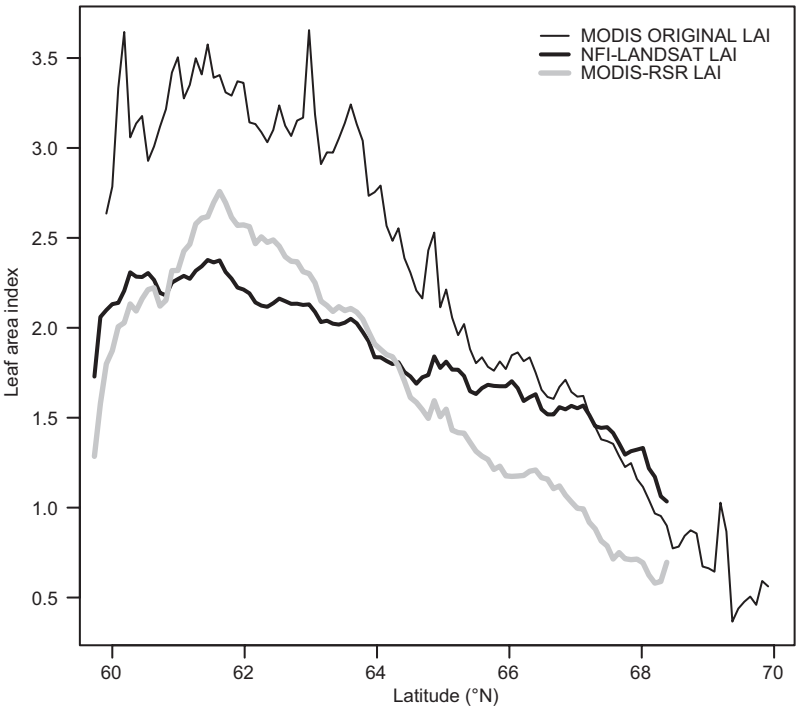

Fig. 4. Latitudinal averages of Landsat-NFI LAI, MODIS-RSR LAI and original MODIS LAI product plotted against the latitude.

NFI-LAI and other pixel properties, such as land use fractions in the MODIS grid. Linear regression calculated using the whole data set showed, that the most significant variables explaining the difference between MODIS-RSR LAI and Landsat-NFI LAI were standard deviation of Landsat-NFI LAI (relative to the average LAI) in the MODIS pixel, deciduous trees in the MODIS pixel, and the latitude (Table 5). Forest fraction was excluded from the regression analysis as its distribution was strongly skewed.

As terrestrial LAI was not measured in the NFI, we assessed our NFI-based LAI estimates by fitting them with the Landsat-based RSR (Fig. 6), and by comparing the results with similar fits for terrestrial LAI and the Landsat-based

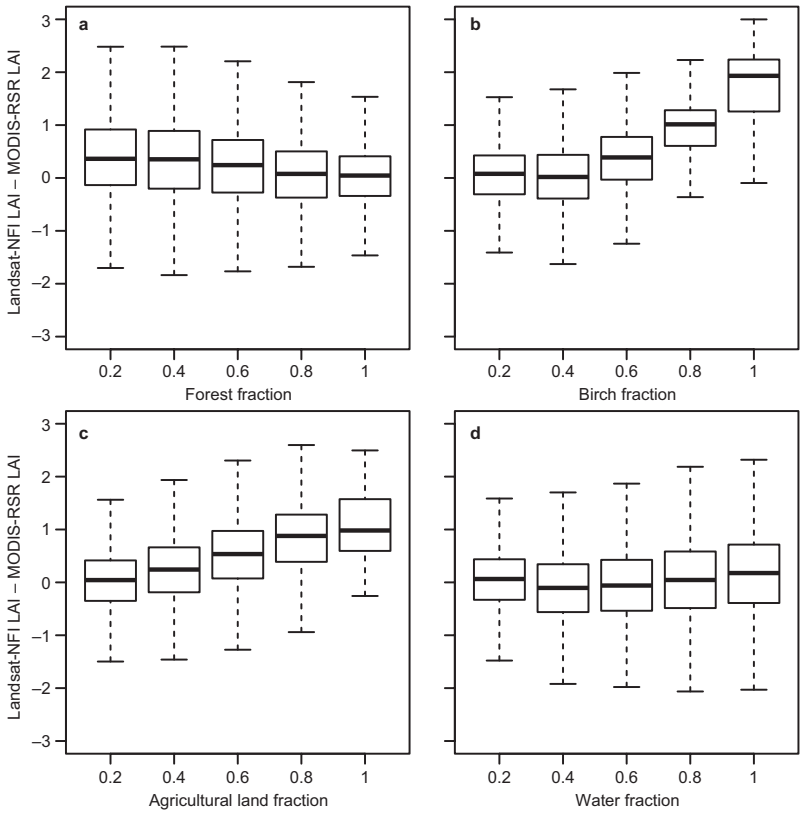

Fig. 5. Box-and-whiskers plots of differences between Landsat-NFI LAI and MODIS-RSR LAI classified by fraction of (**a**) forests, (**b**) birch dominance, (**c**) agricultural land, and (**d**) water in the MODIS pixel. Land use classes are from MS-NFI. Minimum, 1st quantile, median, 3rd quantile and maximum are shown.

RSR from Stenberg *et al*. (2004, 2008). When selecting the NFI plots located in the 30-km radius of these study areas (Scots pine dominated area in Puumala, Norway spruce dominated area in Suonenjoki), a linear regression between LAI and the Landsat-based RSR produced fits close to those obtained by Stenberg *et al*. (2004) especially for Scots pine dominated plots (Fig. 7). Further, effect of seasonal variation in the RSR-based LAI estimates was analyzed by examining overlapping Landsat 5 TM images captured in the early and late summer in the same year, where a shift in the RSR (and therefore in LAI) was detected along the growing season (not shown).

Reliability of *k*-NN imputations was assessed using leave-one-out cross validation based on basal area estimates, as these were measured directly in the field, contrary to the LAI estimates. The LOOC analysis showed that the differences in the RMSE (50.5% for mineral soil plots, 52.8% for peatlands) or bias (1.0% for mineral soils, 0.8% for peatlands) of basal area imputations between the different areas in Finland were not large. The detailed results of the LOOC analysis are presented in Appendix.

Table 5. Linear regression applied to MODIS-RSR LAI and Landsat-NFI LAI (r^2 = 0.61, n = 748017).

	Estimate	SE	t	Pr(>|t|)
Intercept	10.08	0.02	419.33	< 2e–16
LANDSAT_NFI_LAI	0.78	0.00	487.78	< 2e–16
RELATIVE_STDV_LAI	–0.21	0.01	–28.57	< 2e–16
FRACTION_OF_DECIDUOUS TREES	0.07	0.01	8.66	< 2e–16
Y-COORDINATE	–0.0000014	0	–443.52	< 2e–16

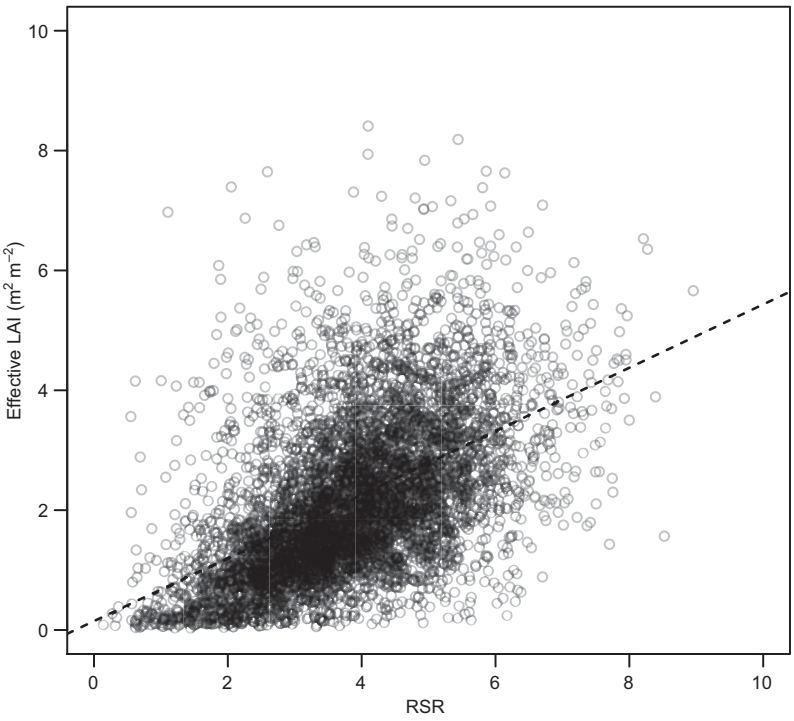

Fig. 6. RSR for NFI plots from Landsat 5 TM plotted against the Landsat-NFI LAI estimates. Only the plots, which were measured in the capture year of the Landsat image are included. LAI_EFF = 0.53RSR + 0.15 (r^2 = 0.26, n = 5673, p < 2.2e–16).

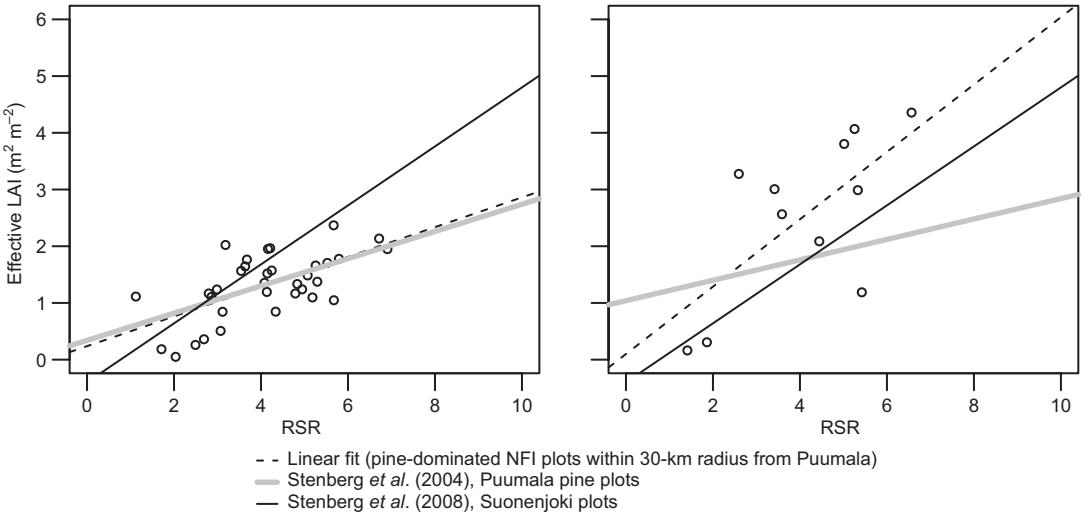

Fig. 7. Left: the RSR from Landsat 5 TM (2007) plotted against effective LAI estimates in the Scots pine dominated NFI plots (plots measured in 2007, 30-km radius from the Puumala study area, > 90% share of Scots pine) (LAI_EFF = 0.26 RSR + 0.24, r^2 = 0.40, n = 34, p = 6.023e-05). Right: the RSR from Landsat 5 TM (2007) plotted against effective LAI estimates in the Norway spruce dominated NFI plots (plots measured in 2007, 30-km radius from the Suonenjoki study area, > 90% share of Norway spruce) (LAI_EFF = 0.60 RSR + 0.10, r^2 = 0.45, n = 11, p = 0.023).

Discussion

In this study, we presented an approach for producing high resolution LAI maps (30 m pixel) based on NFI measurements, allometric equations and Landsat satellite images. Landsat-NFI LAI was compared with coarser resolution MODIS-RSR LAI (500-m pixel), which was produced on

the basis of reflectance of red, infrared and short wave infrared channels of the MODIS satellite image. The analysis was done by comparing Landsat-NFI LAI, which is here average LAI for forest pixels resampled to 500-m resolution, with MODIS-RSR LAI 500-m pixels consisting of > 50% of forests. Even though the country-level averages of Landsat-NFI and MODIS-RSR LAI were somewhat similar, several geographical, seasonal and land-use-related differences between the approaches were detected. Applying moderate or coarse resolution satellite images to estimate environmental parameters seems problematic in areas with fragmented forests and high share of lakes, such as Finland. For example, 500-m pixels consisting of pure forest are very rare especially in southern Finland and pixels consisting entirely of homogeneous forest are even rarer. Even though only the pixels with forest share over 50% (according to CORINE land use classification) were selected for the analysis, our results indicated that the subpixel variation in the land-use affected remarkably the MODIS-RSR LAI estimates.

As terrestrial LAI is not measured in the NFI, we assessed our NFI-based LAI estimates by fitting them with RSR calculated based on the corresponding Landsat 5 TM pixels and comparing it with results of Stenberg *et al*. (2004, 2008). Our fit for Scots pine dominated NFI plots in Puumala was close to that obtained for terrestrial LAI and RSR by Stenberg *et al*. (2004) (Fig. 7), which supports our assumption that the NFI-based LAI estimates were at a reasonable level at least in the southern Finland Scots pine stands. The fit for Norway spruce dominated plots in Suonenjoki was not that well in line with the results of Stenberg *et al*. (2004), but rather close to the fit of Stenberg *et al*. (2008). Majasalmi *et al*. (2013) reported good correlation (0.70) for optical LAI and allometric LAI when using the biomass models of Repola (2008, 2009) to estimate LAI in southern Finland. Also their results were better for Scots pine dominated stands than for stands with other tree species.

The Landsat-NFI LAI and MODIS-RSR LAI estimates differed both geographically and by land-use classes. The MODIS-RSR LAI estimates were higher than Landsat-NFI LAI in the central and eastern parts of Finland. This could be partially explained by the high share of lakes in that area, as the difference tended to increase with an increasing water fraction (Fig. 5). Apart from the pixels with very high water share, the sub-pixel water bodies tend to increase the RSR (Brown *et al*. 2000) through lowering the reflectance values of the bands 3–5. In this kind of areas using a linear LAI:RSR function leads to overestimated LAI values. Differences between MODIS-RSR and Landsat-NFI LAI increased with decreasing proportion of forests in the area, which is obviously due to fact that MODIS-RSR LAI is a result of reflectances from the whole 500-m pixel, which typically include also other land uses than forests. Instead, Landsat-NFI LAI includes only those 30-m pixels, which are defined as forests according to MS-NFI. High proportion of deciduous trees also seemed to increase difference between the MODIS and NFI-based LAI estimates, which can be partly linked to fragmented land-use, as deciduous forests are often found in fertile areas and surroundings of agricultural fields.

When estimating effective LAI as a function of spectral vegetation indices, such as the RSR, it is important to take into account the seasonal effects. For example, the RSR tends to rise quickly during the growing season and drop down in the end of the summer, because it reacts more strongly to the seasonal vegetation changes in the spring and autumn, whereas actual LAI remains more stable during the main growing season (Rautiainen *et al*. 2012). MODIS-RSR LAI was lower than Landsat-NFI LAI in the northern part of Finland, which is likely due to the MODIS image capture time. The image was captured in the beginning of June, when the growing season had not yet properly started in northern Finland. Therefore, MODIS-RSR LAI was likely an underestimate of the average growing season LAI in that region. Further, as the used linear LAI model has a negative intercept, it might lead to close-to-zero or even negative LAI estimates with low RSR values. This problem is also due to the different seasonality of the RSR and LAI, as the linear RSR model used for producing MODIS-RSR LAI was fitted based on an image acquired in late summer (2 August 2003), but applied to the image captured in the beginning of the growing season. The

seasonal variation in the RSR was examined further by comparing the Landsat-based RSR for overlapping Landsat images captured in June and August in 2007. In that case, the RSR (and therefore LAI) were remarkably higher in the late summer than in the beginning of summer. As a conclusion, when applying the existing linear RSR-based LAI functions to satellite images, the applied models should be from the same phase of the growing season as the images. Developing more advanced models for estimating LAI based on spectral vegetation indices and a growing season phase remains as a future task. In our study, the relationship of the Landsat-based RSR and allometrically estimated LAI was rather stable for Scots pine dominated stands, but varied with other tree species in different Landsat images. The RSR:LAI fits with Norway spruce and birch stands were poorer, especially with the images captured in the late summer (not shown). Similar phenomena was discovered by Eklundh *et al*. (2003), who reported that estimating LAI based on the RSR in Sweden was suitable only for coniferous stands. Original MODIS LAI was remarkably higher than LAI from other approaches, which is obviously due to the effects of the understory vegetation (Tian *et al*. 2002, Wang *et al*. 2004). This also explains smaller differences in LAI estimates in the northernmost latitudes, where deciduous trees and understory vegetation were still entering their growing season.

The Landsat-NFI LAI estimation chain also contains several sources of uncertainty. Firstly, the biomass models have certain geographical and species-specific weaknesses: e.g., Majasalmi *et al*. (2013) reported failures to estimate birch leaf biomass in certain cases when using Repola's models. This failure might also be partially due to small sample size behind the birch foliage model and due to the fact that sampling was concentrated in southern Finland. Further, Repola's Scots pine models are based on measurements in the autumn, which might cause underestimations of the average needle biomasses during the growing season, as reported by Majasalmi *et al*. (2013). Secondly, Landsat-NFI LAI was estimated based on leaf biomasses assuming constant species-specific SLA for shade and light leaves, even though in reality SLA varies inside the canopy and during the growing season (e.g. Sellin and Kupper 2006). Consequently, we divided the canopy biomass of dense coniferous forests into shadow and sun needles (canopy cover > 50%–70%). The biomass located below the median tree's crown base was applied with the shadow needle's specific leaf area, and the rest was treated as sun needles. Estimated uncertainty for Scots pine LAI using this method is ±8.5% of the mean LAI estimate, as applying sun SLA for the whole canopy produces 17% lower LAI, than using shadow SLA. For Norway spruce, the corresponding uncertainty interval is ±13.5% of the mean LAI estimate.

The Landsat-NFI LAI estimates were produced by imputing the NFI-based LAI estimates to grid level using *k*-NN imputation. Reliability of imputation was validated by comparing the field-measured and imputed basal areas in the NFI plots using the LOOC procedure. There were no remarkable geographical differences in the reliability of *k*-NN imputation, with exception of three regions from which the reference data on peatland plots was too scarce (< 100 plots) to produce reliable imputation. The RMSE of imputations was high (around 50%), but of the same level as reported in the previous studies using satellite image bands as explanatory variables (e.g., Tuominen 2007). In this study we applied $k = 1$, which, as mentioned before, retains the full variation of the field reference data in the estimates. On the other hand, this method increases a risk of getting biased estimates for certain cells when the reference data set contains some anomalies. Typically when using large reference data sets, such as NFI plots, the estimation accuracy tends to improve when increasing the value of k in a range 1–20 (e.g., Tokola *et al*. 1996, Nilsson 1997). However, the higher the value of k, the more averaging occurs in the estimates. Thus, while the optimal value of k is a trade-off between the accuracy of the estimates and proportion of the original variation retained in the estimates, a higher value of k would probably have resulted in locally more accurate estimates. Further improvement in the *k*-NN estimation accuracy might be achieved by, e.g., correcting the spectral values of satellite images by taking into account the effect of terrain slope and aspect on the solar illumina-

tion angle (e.g. Tomppo 1992). Another way of improving the local estimation accuracy would be the use of coarse-scale auxiliary data such as information on local tree species proportions or dominance, which can be applied as additional information for guiding the selection of nearest neighbors (e.g. Tomppo *et al*. 2008, 2012).

Even though the country-level averages of MODIS-RSR LAI and Landsat-NFI LAI were in line with each other in Finland, their regional differences might lead to significantly different carbon production estimates at a country level, as models for estimating gross primary production (GPP), net primary production (NPP) and net ecosystem exchange (NEE) rely both on LAI and local weather conditions. Therefore, further evaluation of national GPP, NPP and NEE differences with different LAI products are needed to evaluate their effects on forest carbon sinks (*see* Peltoniemi *et al*. 2015).

Conclusions

Linking NFI data with Landsat satellite images for *k*-NN imputation offers straightforward method to produce high resolution LAI maps for large region ecological applications. In addition to its high resolution, one of the main advantages of this method is that contrary to RSR-based LAI estimations, no atmospheric correction is required, as *k*-NN imputation is applied separately to each image. However, methods for estimating biomass and LAI, especially in deciduous forests and in the north, should still be improved.

To estimate forest carbon balance correctly at a country level, it is essential to use LAI maps, which are reliable both regionally and at the country level. Using coarse and moderate resolution images for estimating ecological parameters such as LAI for Finland or other highly fragmented areas seems problematic in that sense. Mixing the forest reflectance with that of water, agricultural land or some other land use can be avoided by using higher resolution images, such as Landsat, or by processing the images with correction algorithms aiming to remove effects of e.g. water bodies. Estimating LAI based on the RSR or some other spectral vegetation index is reasonable alternative, when the satellite images are applied with species-specific models, which are from the same phase of the growing season as the image concerned. As the RSR:LAI relationship seems to work best for the Scots pine dominated stands, developing better methods for other tree species LAI estimation remains as a future task.

Acknowledgements: This study was partially funded by the Carb-Bal project at Finnish Forest Research Institute (Academy of Finland, no. 128018) and the University of Helsinki (Academy of Finland, no. 128236) and partially by the CLIMFORISK (Climate change induced drought effects on forest growth and vulnerability) project (no. LIFE09 ENV/FI/000571). We thank the Finnish Forest Research Institute for providing the NFI data, and the Finnish Environment Institute for conducting atmospheric correction to the MODIS images. In addition, we are grateful to Dr. Ali Nadir Arslan from the Finnish Meteorological Institute and Dr. Kalle Eerikäinen from the Finnish Forest Research Institute for their help and cooperation in the Carb-Bal project. In addition, Prof. Erkki Tomppo and For. Eng. Jouni Peräsaari from the Finnish Forest Research Institute are acknowledged for pre-processing Landsat images for the major part of the study area.

References

Bréda N.J.J. 2003. Ground-based measurements of leaf area index: a review of methods, instruments and current controversies. *Journal of Experimental Botany* 54: 2403–2417.

Brown L., Chen J.M., Leblanc S.G. & Cihlar J. 2000. A shortwave infrared modification to the simple ratio for LAI retrieval in boreal forests: an image and model analysis. *Remote Sensing of Environment* 71: 16–25.

Cajander A.K. 1925. Metsätyyppiteoria. *Acta Forestalia Fennica* 1: 1–84.

Chavez P.S. 1996. Image-based atmospheric corrections — revisited and improved. *Photogrammetric Engineering and Remote Sensing* 62: 1025–1036.

Chen J.M., Rich P.M., Gower S.T., Norman J. & Plummer S. 1997. Leaf area index of boreal forests: Theory, techniques, and measurements. *Journal of Geophysical Research* 102: 29429–29443.

Clevers J.G.P.W. 1988. The derivation of a simplified reflectance model for the estimation of leaf area index. *Remote Sensing of Environment* 25: 53–69.

Crookston N.L. & Finley A.O. 2008. yaImpute: an R package for kNN imputation. *Journal of Statistical Software* 23: 1–16.

Curran P.J & Steven M.D. 1983. Multispectral remote sensing for the estimation of green leaf area index [and discussion]. *Philosophical Transactions of the Royal Society of London* 309: 257–270.

Eerikäinen K. 2009. A multivariate linear mixed-effects model for the generalization of sample tree heights and crown ratios in the Finnish National Forest Inventory. *Forest Science* 55: 480–493.

Eklundh L., Hall K., Eriksson H., Ardö J. & Pilesjö P. 2003. Investigating the use of Landsata thematic mapper data for estimation of forest leaf area index in southern Sweden. *Canadian Journal of Remote Sensing* 29: 349–362.

Härkönen S., Lehtonen A., Eerikäinen K., Peltoniemi M. & Mäkelä A. 2011. Estimating forest carbon fluxes for large regions based on process-based modelling, NFI data and Landsat satellite images. *Forest Ecology and Management* 262: 2364–2377.

Heiskanen J., Rautiainen M., Korhonen L., Mõttus M. & Stenberg P. 2011. Retrieval of boreal forest LAI using a forest reflectance model and empirical regressions. *International Journal of Applied Earth Observation and Geoinformation* 13: 595–606.

Heiskanen J., Rautiainen M., Stenberg P., Mõttus M., Vesanto V.H., Korhonen L. & Majasalmi T. 2012. Seasonal variation in MODIS LAI for a boreal forest area in Finland. *Remote Sensing of Environment* 126: 104–115.

Irish R.R. Barker J.L. Goward S.N. & Arvidson T. 2006. Characterization of the Landsat-7 ETM+ Automated Cloud-Cover Assessment (ACCA) Algorithm. *Photogrammetric Engineering and Remote Sensing* 72: 1179–1188.

Irish R.R. 2000. Landsat 7 automatic cloud cover assessment. *Proceedings of SPIE* 4049: 348–355.

Korhonen L., Korpela I., Heiskanen J. & Maltamo M. 2011. Airborne discrete-return LiDAR data in the estimation of vertical canopy cover, angular canopy closure and leaf area index. *Remote Sensing of Environment* 115: 1065–1080.

Lee H., Slatton K.C., Roth B.E. & Cropper W.P. 2009. Prediction of forest canopy light interception using three-dimensional airborne LiDAR data. *International Journal of Remote Sensing* 30: 189–207.

Lefsky M.A., Cohen W.B., Acker S.A., Parker G.G., Spies T.A. & Harding D. 1999. Lidar remote sensing of the canopy structure and biophysical properties of Douglas-fir western hemlock forests. *Remote Sensing of Environment* 70: 339–361.

Lintunen A., Sievänen R., Kaitaniemi P. & Perttunen J. 2011. Models of 3D crown structure for Scots pine (*Pinus sylvestris*) and silver birch (*Betula pendula*) grown in mixed forest. *Canadian Journal of Forest Research* 41: 1779–1794

Majasalmi T., Rautiainen M., Stenberg P. & Lukeš P. 2013. An assessment of ground reference methods for estimating LAI of boreal forests. *Forest Ecology and Management* 292: 10–18.

Myneni, R.B. Nemani R.R. & Running S.W. 1997. Estimation of global leaf area index and absorbed PAR using radiative transfer models. *IEEE Transactions on Geoscience and Remote Sensing* 35: 1380–1393.

Myneni R.B., Hoffman S., Knyazikhin Y., Privette J.L., Glassy J., Tian Y., Wang Y., Song X., Zhang Y., Smith G.R., Lotsch A., Friedl M., Morisette J.T., Votava P., Nemani R.R. & Running S.W. 2002. Global products of vegetation leaf area and fraction absorbed PAR from year one of MODIS data. *Remote Sensing of Environment* 83: 214–231.

Nilsson M. 1997. Estimation of forest variables using satellite image data and airborne lidar. *Acta Universitatis Agriculturae Sueciae, Silvestria* 17: 1–84.

Palmroth S., Berninger F., Nikinmaa E., Lloyd J., Pulkkinen P. & Hari P. 1999. Structural adaptaion rather than water conservation was observed in Scots pine over a range of wet to dry climates. *Oecologia* 121: 302–309.

Parviainen T. 1999. *Sekametsiköiden koivujen biomassan ja latvusrakenteen selvittäminen elintoimintoihin perustuvia kasvumalleja varten*. M.Sc. thesis, Department of Forest Ecology, University of Helsinki.

Peltoniemi M., Markkanen T., Härkönen S., Muukkonen P., Thum T., Aalto T. & Mäkelä A. 2015. Consistent estimates of gross primary production of Finnish forests — comparison of estimates of two process models. *Boreal Env. Res*. 20: 196–212.

Rahman H. & Dedieu G. 1994. SMAC: a simplified method for the atmospheric correction of satellite measurements in the solar spectrum. *International Journal of Remote Sensing* 15: 123–143.

Rautiainen M., Heiskanen J. & Korhonen L. 2012. Seasonal changes in canopy leaf area index and MODIS vegetation products for a boreal forest site in central Finland. *Boreal Environment Resesarch* 17: 72–84.

Repola J. 2008. Biomass equations for birch in Finland. *Silva Fennica* 42: 605–624.

Repola J. 2009. Biomass equations for Scots pine and Norway spruce in Finland. *Silva Fennica* 43: 625–647.

Sellin A. & Kupper P. 2006. Spatial variation in sapwood area to leaf area ratio and specific leaf area within a crown of silver birch. *Trees* 20: 311–319.

Song C., Woodcock C.E., Seto K.C., Lenney M.P. & Macomber S.A. 2001. Classification and change detection using landsat TM data: when and how to correct atmospheric effects. *Remote Sensing of Environment*. 75: 230–244.

Stenberg P. 1996. Correcting LAI-2000 estimates for the clumping of needles in shoots of conifers. *Agricultural and Forest Meteorology* 79: 1–8.

Stenberg P., Smolander H., Sprugel D. & Smolander S. 1998. Shoot structure, light interception and distribution of nitrogen in an *Abies amabilis* canopy. *Tree Physiology* 18: 759–767.

Stenberg P., Kangas T., Smolander H. & Linder S. 1999. Shoot structure, canopy openness, and light interception in Norway spruce. *Plant, Cell & Environment* 22: 1133–1142.

Stenberg P., Palmrot S., Bond B.J., Sprugel D.G. & Smolander H. 2001. Shoot structure and photosynthetic efficiency along the light gradient in a Scots pine canopy. *Tree Physiology* 21: 805–814.

Stenberg P., Rautiainen M., Manninen T., Voipio P. & Smolander H. 2004. Reduced simple ratio better than NDVI for estimating LAI in Finnish pine and spruce stands. *Silva Fennica* 38: 3–14.

Stenberg P., Rautiainen M., Manninen T., Voipio P. & Mõttus M. 2008. Boreal forest leaf area index from optical sat-

ellite images: model simulations and empirical analyses using data from central Finland. *Boreal Environment Research* 13: 433–443.

Tokola T., Pitkänen J., Partinen S. & Muinonen E. 1996. Point accuracy of a non-parametric method in estimation of forest characteristics with different satellite materials. *International Journal of Remote Sensing* 17: 2333–2351.

Tomppo E. 1992. Satellite image aided forest site fertility estimation for forest income taxation. *Acta Forestalia Fennica* 229: 1–70.

Tomppo E., Haakana M., Katila M. & Peräsaari J. 2008. Multisource national forest inventory — methods and applications. *Managing Forest Ecosystems* 18: 1–374.

Tomppo E., Katila M., Mäkisara K. & Peräsaari J. 2012. The multi-source national forest inventory of Finland — methods and results 2007. *Working Papers of the Finnish Forest Research Institute* 227: 1–233.

Tuominen S. 2007. Estimation of local forest attributes, utilizing two-phase sampling and auxiliary data. *Dissertationes Forestales* 41: 1–46.

Törmä M., Haakana M., Hatunen S., Härmä P., Kallio M., Katila M., Kiiski T., Mäkisara K., Peräsaari J., Piepponen H., Repo R., Teiniranta R. & Tomppo E. 2008. Finnish Corine 2006-project: determining changes in land cover in Finland between 2000 and 2006. *Proceedings of SPIE* 7110: 1–12.

Appendix. Leave-one-out-cross validation for basal area (BA, m^2 ha^{-1}) estimates for different images and soil types for Finland.

	Path/row	Bias	Bias%	RMSE	RMSE%	Average measured BA	*n*	Percentage of sample plots in the area
Mineral soils								
	188/15	0.2	1.3	8.9	50.6	17.7	1608	60.8
	188/16	0.1	0.3	10.1	51.9	19.4	3005	76.3
	188/17	0.2	1.2	10.2	50.6	20.1	3181	84.3
	188/18	0.2	1.2	10.7	50.7	21	1019	86.6
	190/14	0.2	1.2	7.4	48.2	15.4	1349	61.5
	190/15	0.1	0.5	9.1	54	16.8	1384	50.0
	190/16	0.2	1.2	9.2	50.1	18.4	2595	65.8
	190/17	0.2	1.2	10.4	51.6	20.2	2753	77.0
	190/18	0.3	1.5	10.5	51.3	20.5	907	86.5
	191/11–12	–0.1	–0.8	5.3	49.2	10.7	473	96.7
	186/16–18	0.3	1.4	10.5	52.7	19.9	3629	76.6
	191/16	0.3	1.5	9	50.2	18	1655	62.4
	191/18	0.3	1.5	12.3	57.6	21.4	438	93.4
	190/12–13	0.1	1.2	5.7	50.4	11.3	1523	87.5
	193/13	0	–0.3	6.2	51.1	12.1	523	75.0
	193/12	0.3	2.4	4.9	42.6	11.4	672	93.5
	188/15	0.2	1.4	7.6	46.1	16.4	1300	62.5
	188/14	0.1	0.4	7.6	49.5	15.4	1264	79.0
Peatlands								
	188/15	0.1	0.6	7.3	45.8	16	1038	39.2
	188/16	0.2	0.9	9.1	49.7	18.4	935	23.7
	188/17	0.5	2.3	8.9	45.2	19.8	593	15.7
	188/18	0.5	2.4	12.6	58.7	21.5	158	13.4
	190/14	0.2	1.2	7.6	52.3	14.6	843	38.5
	190/15	0.4	2.6	7.6	48.1	15.7	1386	50.0
	190/16	0.3	2.0	8.4	50.3	16.6	1347	34.2
	190/17	0.2	0.9	9	47.6	18.9	823	23.0
	190/18	0.5	2.4	12.4	57.8	21.5	142	13.5
	191/11–12	0.5	5.4	5.4	57.7	9.3	16	3.3
	186/16–18	0.2	0.9	9.1	49.9	18.2	1110	23.4
	191/16	0.1	0.6	8.7	50.3	17.3	996	37.6
	191/18	–2.3	–10.0	13.2	56.9	23.2	31	6.6
	190/12–13	0.5	4.3	6.6	54	12.3	218	12.5
	193/13	0.3	2.5	7.7	64.4	12	174	25.0
	193/12	–0.3	–2.2	6.5	56.1	11.6	47	6.5
	188/15	0	–0.3	6.5	46.8	13.8	781	37.5
	188/14	–0.2	–1.9	7.4	58.3	12.6	336	21.0